Gd 3+ Complexes for MRI Detection of Zn 2+ in the Presence of Human Serum Albumin: Structure–Activity Relationships

Kyangwi Malikidogo, Manon Isaac, Adrien Uguen, Jean-François Morfin, Gyula Tircsó, Éva Tóth, Celia Bonnet

Gd^{3+} Complexes for MRI Detection of Zn^{2+} in the Presence of Human Serum Albumin: Structure-Activity Relationships

Kyangwi P. Malikidogo,[a,†] Manon Isaac,[a] Adrien Uguen,[a] Jean-François Morfin,[a] Gyula Tircsó,[b,c] Éva Tóth,[a] Célia S. Bonnet*[,a]

[a] Centre de Biophysique Moléculaire, CNRS UPR 4301, Université d'Orléans, Rue Charles Sadron, F-45071, Orléans 2, France

[b] Department of Inorganic and Analytical chemistry, University of Debrecen, Egyetem tér 1, 4010 Debrecen, Hungary

[c] Le Studium, Loire Valley Institute for Advanced Studies, 1 rue Dupanloup, 45000 Orléans, France

[†] Current address : Département des Sciences et Technologies, Université de Goma, B.P. 204 Goma, R.D. Congo

Abstract

Zn^{2+} responsive MRI contrast agents are typically composed of a Gd-chelate conjugated to a Zn^{2+} binding moiety via a linker, and allow for Zn^{2+} detection in the presence of Human Serum Albumin (HSA). In order to decipher key parameters driving their Zn^{2+}-dependent MRI response, we designed a pyridine-based ligand, PyAmC2mDPA, and compared the properties of GdPyAmC2mDPA to those of analogue complexes with varying Gd-core, Zn-binding moiety or linker size. Stability constants determined by pH-potentiometry show good selectivity of PyAmC2mDPA for Gd^{3+} (Log K_{Gd} = 16.27) vs Zn^{2+} (Log K_{Zn} = 13.58), and prove that our modified Zn^{2+}-binding DPA moiety prevents the formation of previously observed dimeric species. Paramagnetic Relaxation Enhancement measurements indicate at least three sites available for GdPyAmC2mDPA binding on the HSA, and a twofold affinity increase when Zn^{2+} is present (K_D = 170 µM vs K_{DZn} = 60 µM). Fluorescence competition experiments evidence the higher affinity for site II and the importance of both the Zn-binding part and the Gd-core to generate enhanced HSA affinity in the presence of Zn^{2+}. Finally, the analysis of Nuclear Magnetic Relaxation Dispersion (NMRD) data suggests significantly increased rigidity for the Zn^{2+}-bound system which is responsible for the Zn^{2+}-dependent relaxivity response.

Introduction

Zinc is the second most abundant transition metal in the body after iron[1], involved in many biological processes. It is not redox active, and mainly bound to proteins controlling gene transcription or metalloenzyme functions[2], but it is also a signalling ion relevant in pathways of the immune system[3], or in fertilization processes[4] for example. As for other physiological ions, zinc concentration is tightly regulated, and misregulations in its homeostasis are implicated in various diseases such as cancers,[5] neurodegenerative diseases[6] or diabetes[7].

Therefore, *in vivo,* non-invasive imaging of Zn^{2+} would be helpful, both for early diagnosis of pathologies where Zn^{2+} is implicated and for fundamental biomedical research. Among *in vivo* imaging modalities, Magnetic Resonance Imaging (MRI) stands out with an exceptional spatial resolution, and gives the most precise information at the macroscopic level. In order to compensate for the low sensitivity of MRI, contrast agents (CAs) can be injected. These are commonly Gd^{3+} complexes based on DOTA (1,4,7,10-tetraazacyclododecan-1,4,7,10-tetraacetic acid) or DTPA (diethylenetriamine-pentaacetic acid), and upon modification, these contrast agents can be rendered responsive to bioactive molecules, such as Zn^{2+}.[8] Typically, such responsive CAs are composed of three parts: (1) the Gd^{3+}-binding moiety that must be thermodynamically stable and kinetically inert; (2) the Zn^{2+}-binding part, and (3) a linker between the two. Two main mechanisms can be utilised to modulate the efficacy of a contrast agent (called relaxivity) upon interaction with Zn^{2+}: (1) modification of the number of water molecules coordinated to Gd^{3+}, or (2) modification of the rotational motion of the complex, related to molecular size and rigidity.[9] The rotational dynamics can be further modulated by the Zn^{2+}-dependent variation of the probe affinity for a given protein, typically Human Serum Albumin (HSA).

The field of Zn^{2+}-responsive CAs has witnessed important development in the last fifteen years, particularly since the onset of *in vivo* applications.[10] Early detection of prostatic cancer[11] or diabetes[12] using such probes proved for the first time the feasibility of *in vivo* Zn^{2+} mapping. Interestingly, the most successful Zn^{2+} responsive contrast agents provide a Zn^{2+}-dependent relaxivity change in the presence of HSA, the most abundant protein in the blood.[13]

HSA is composed of three homologous domains, each composed of two subdomains.[14] HSA can bind various endogenous compounds such as fatty acids, metals, heme, NO, but also drugs, altering their pharmacokinetics properties.[15] Small molecules usually bind to two different pockets: Sudlow's site I, a hydrophobic cavity of the subdomain IIA which accommodates bulky heterocyclic anions, and Sudlow's

site II located in the subdomain IIIA, which is preferred for aromatic carboxylates with an extended conformation. HSA also possesses four metal binding sites, the N-terminal site, the site at the reduced Cys34, the multi-metal binding site A (MBS) at the I/II interdomain contact region, and the non-localized site B. The MBS has the highest affinity for the Zn^{2+}, in the 100 nM range, while site B has an affinity in the µM range.[16] The MBS binds Zn^{2+} with two histidines and one aspartate, completed with one water molecule.[17] Due to its high affinity (log K_{HSA-Zn} = 7.53),[18] 75-85% of the 10-18 µM total plasma zinc concentration[19] is bound to HSA. Therefore, Zn^{2+} responsive CAs have multiple possibilities to interact with HSA, which are not easy to predict.

We have previously developed a series of pyridine-based ligands for Gd^{3+} complexation.[20-21] **Py** (Scheme 1) is attractive because its Gd^{3+} complex has good MRI efficacy (two water molecules in the first coordination sphere of Gd^{3+}), combined with good thermodynamic stability and kinetic inertness,[22] without acute or long-term toxicity.[21] We have derivatized this system to append a Zn^{2+}-binding unit, a derivative of AMPA (2-aminomethyl)pyridine-N-monoacetic acid) (**L1/L2/L3**, Scheme 1), which has nanomolar affinity for Zn^{2+} (log K = 7.6).[23] This AMPA derivative was previously used by Nagano *et al.* linked to a DTPA-based complex which responds to Zn^{2+} by a modification of the water exchange rate.[24] We showed that (1) the presence of the amide is necessary to have enough selectivity for Gd^{3+} vs Zn^{2+} (**L1** vs **L2/L3**) and (2) the Gd^{3+} complexes of this first generation of ligands (**L2/L3**) provide a relaxivity response to Zn^{2+} through the formation of $(GdL)_2Zn$ dimers.[25]
By modifying both the Zn^{2+}- and the Gd^{3+}-binding part (**PyC4mDPA,** Scheme 1), a monotonic relaxivity variation could be achieved upon Zn^{2+} addition, in the presence of HSA. This allowed for *in vitro* Zn^{2+} quantification using a cocktail of the Gd^{3+} and the $^{165}Er^{3+}$ complex.[26] **GdPyC4mDPA** proved also useful to elucidate the molecular bases underlying the *in vivo* MRI response of such systems to variations in the Zn^{2+} concentration.[27]
In the aim of further understanding the parameters governing stability, HSA affinity, relaxation properties and Zn^{2+}-dependent relaxometric behaviour in this family of Zn^{2+} responsive MRI probes, we report here a novel analogue, **PyAmC2mDPA** (Scheme 1) which has the same Gd^{3+}-binding part as the first generation of ligands **L2** and **L3**, and the same Zn^{2+}-binding unit as **PyC4mDPA**. **PyAmC2mDPA** and **PyC4mDPA** have different charge, which might affect the protein binding properties, as well as the potential of the Gd^{3+} complex to change its hydration number upon interacting with Zn^{2+}. In order to better rationalize the findings, two model compounds, **ZP1** and **ZP2** (Scheme 1) which mimic the Zn^{2+}-binding moieties, have been also synthesized and

involved in these studies. We have performed potentiometric titrations to assess the stability and selectivity of **PyAmC2mDPA** for Ln^{3+} vs cations present in the physiological milieu. We demonstrate that the Zn^{2+}-binding unit of this ligand prevents dimerization in the presence of Zn^{2+} and that HSA-binding allows for Zn^{2+} detection *in vitro*, with a maximum relaxivity response at medium magnetic field. We have investigated in detail the interaction between the complexes and HSA using relaxometric and fluorescence measurements. Combined with the variable-temperature NMRD profiles in the presence and in the absence of Zn^{2+} and HSA, this full characterisation helps decipher the key factors involved in the relaxivity response to Zn^{2+} and gives valuable insights for further improvement of Zn^{2+}-responsive MRI probes.

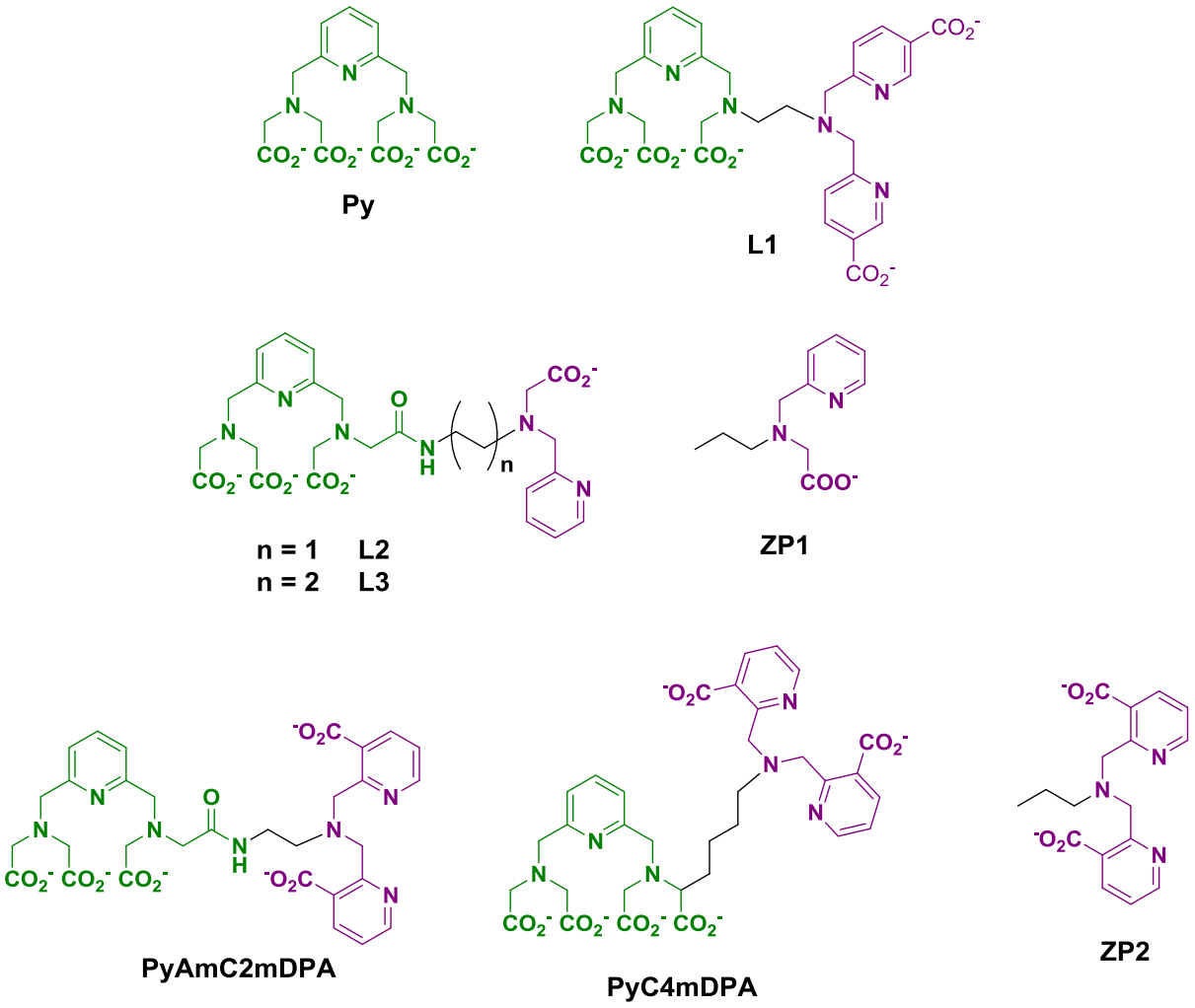

Scheme 1: Chemical structures of the ligands discussed in this work. The Gd^{3+}- and Zn^{2+}-binding parts are indicated respectively in green and in violet.

Experimental Section

General remarks

$ZnCl_2$, $GdCl_3$, Hepes and fatty acid free albumin from human serum were purchased from Sigma Aldrich. Synthesis and characterization of the compounds discussed in this work is described in the Supporting Information.

Liquid sample preparation

The ligand concentrations were determined by adding an excess of zinc solution to a ligand solution and titrating the metal excess with standardized Na_2H_2EDTA in urotropine buffer (pH 5.6–5.8) in the presence of Xylenol Orange or Eriochrome Black T, or Murexide as indicators. The concentration of the metal solutions was determined similarly by complexometric titrations. The complexes were prepared by mixing 1 eq. of L, with 1 eq. of Gd^{3+}, and the pH was adjusted to 7.4 either with a buffered solution or by adding KOH or HCl to the solution. The absence of free Gd^{3+} was checked by the Xylenol orange test. The concentrations of Gd^{3+}-containing solutions were also checked both by ICP-MS and BMS measurements when possible.

Potentiometric studies

Carbonate-free 0.1 M KOH and 0.1 M HCl were prepared from Fisher Chemicals concentrates. Potentiometric titrations were performed in 0.1 mol. L^{-1} aqueous KCl under nitrogen atmosphere and the temperature was controlled to 25±0.1 °C with a circulating water bath. The p[H] (p[H] = -log[H+], concentration in molarity) was measured in each titration with a combined pH glass electrode (Metrohm) filled with 3M KCl and the titrant addition was automated by use of a 702 SM titrino system (Metrohm). The electrode was calibrated in hydrogen ion concentration by titration of HCl with KOH in 0.1 M electrolyte solution.[28] A plot of meter reading versus p[H] allows the determination of the electrode standard potential (E°) and the slope factor (f). Continuous potentiometric titrations with HCl and KOH 0.1 M were conducted on aqueous solutions containing 5 mL of L 3.23 mM in KCl 0.1 M, with 2 minutes waiting between successive points. The titrations of the metal complexes were performed with the same ligand solutions containing 1 or 2 equivalents of metal cation, with 2 minutes waiting time between 2 points. Experimental data were refined using the computer program Hyperquad 2008.[29] All equilibrium constants are concentration quotients rather than activities and are defined as:

$$K_{mhl} = \frac{[M_m L_l H_h]}{[M]^m [L]^l [H]^h}$$

The ionic product of water at 25 °C and 0.1 molL-1 ionic strength is pKw = 13.77.[30] Fixed values were used for pKw, ligand acidity constants and total concentrations of metal, ligand and acid. All values and errors (one standard deviation) reported are at least the average of three independent experiments.

NMR spectroscopy

The ^{1}H, ^{13}C and complementary experiments (COSY, HSQC and HMBC) NMR spectra were recorded on a Bruker Advance III HD Spectrometer at 298 K using a 5 mm BBFO probe. ^{1}H and ^{13}C spectra were obtained respectively at 600 MHz and 150 MHz.

UV-visible spectroscopy:

UV-visible absorption spectra were recorded on a V 670 JASCO UV-Vis/NIR Spectrophotometer in the range λ = 350-875 nm with data steps of 1 nm, with a 1 cm path length. Measurements were performed at 298 K and in KCl 1 M. Out-of-cell (batch) samples were prepared containing the ligand (2.5 mM for **PyAmC2mDPA**, 1.56 mM for **PyC4mDPA** and 3 mM for **ZP2**) and 1 or 2 equivalents of Cu^{2+} with various HCl concentrations.

Relaxometric measurements

Proton NMRD profiles were recorded on a Stelar SMARTracer Fast Field Cycling relaxometer (0.01-10 MHz) and a Bruker WP80 NMR electromagnet adapted to variable field measurements (20-80 MHz) and controlled by a SMARTracer PC-NMR console. The temperature was monitored by a VTC91 temperature control unit and maintained by a gas flow. The temperature was determined by previous calibration with a Pt resistance temperature probe. The longitudinal relaxation rates ($1/T_1$) were determined in water.

Luminescent measurements

Fluorescence spectra were recorded on an Agilent Cary Eclipse Fluorescence spectrophotometer with the following settings: excitation at 260 nm and emission scanning between 400 and 700 nm with an emission filter 360-1100nm, slit widths 5 nm for excitation and emission wavelengths, at 313K. The mixtures in a 500 µL quartz cuvette with a 2x10 mm path length were incubated for 3 min before the measurements were taken. To determine the

affinity of dansylated aminoacids for HSA, various amounts of dansylaminoacid were added to a solution of [HSA] = 5 µM in 10 mM HEPES buffer, pH 7.2. For the displacement experiments, various amount of the different compounds were added to a solution of [HSA] = 5 µM and [dansylglycine] = 10µM in 10 mM HEPES buffer pH 7.2. All spectra were normalized, then imported in HypSpec 2014 (Hyperquad suite). All titration were fitted taking into account two equilibria: HSA + DslAA = HSA-DslAA and HSA + GdL = HSA-GdL ($Kd_{HSA-GdL}$). The formation constant of HSA-dansylglycine was set at $\beta_{HSA-DslGly}$ = 5.47 and for HSA-dansylarginine at $\beta_{HSA-DslArg}$ =3.9, and the emission spectra of the dansylglycine in 10 mM HEPES buffer pH 7.2 was recorded and set in HypSpec.

Europium luminescence lifetimes were recorded on an Agilent Cary Eclipse Fluorescence spectrophotometer by recording the decay of the emission intensity at 616 nm, following an excitation at 272 nm. Measurements were performed in H_2O and D_2O solutions. The settings were as follow: gate time: 0.1 ms; delay time: 0.1 ms; flash count: 1; Total decay time: 10 ms; 100 cycles; PMT detector: 800 mV. At least three decay curves were collected for each sample, all lifetimes were analyzed as monoexponential decays, and it was also checked that direct excitation of the metal at 396 nm gave similar results. The reported lifetimes are an average of at least three measurements.

Results and Discussion

Synthesis of ligands

The ligand **PyAmC2mDPA** was synthetized in 8 steps (Scheme 2). First the Gd^{3+} binding motif was prepared starting from 2,6-bis(bromomethyl)pyridine which was reacted statistically with diethyl iminodiacetate to afford compound **1**. Then, another statistical reaction was performed with an excess of glycine ethyl ester hydrochloride to lead to the derivative **2**. The linker was then introduced by *N*-alkylation of the secondary amine function with compound **3**, which was previously obtained by acylation of the commercial *N*-Boc ethylenediamine with chloroacetyl chloride. A cyclization occurred during this *N*-alkylation reaction and the 2,6-piperazinedione derivative **4** was obtained as major product. Indeed, it could be explained by high reactivity towards lactamization due to the thermodynamically favorable formation of a 6-membered ring. After the cleavage of the carbamate protecting group under acidic conditions, the modified DPA unit was built by di-*N*-alkylation with product **6**, previously prepared by radical bromination of methyl-2-methylnicotinate. The ester functions and the

piperazinedione cycle of compound **7** were hydrolysed in basic conditions to finally lead to ligand **PyAmC2mDPA**.

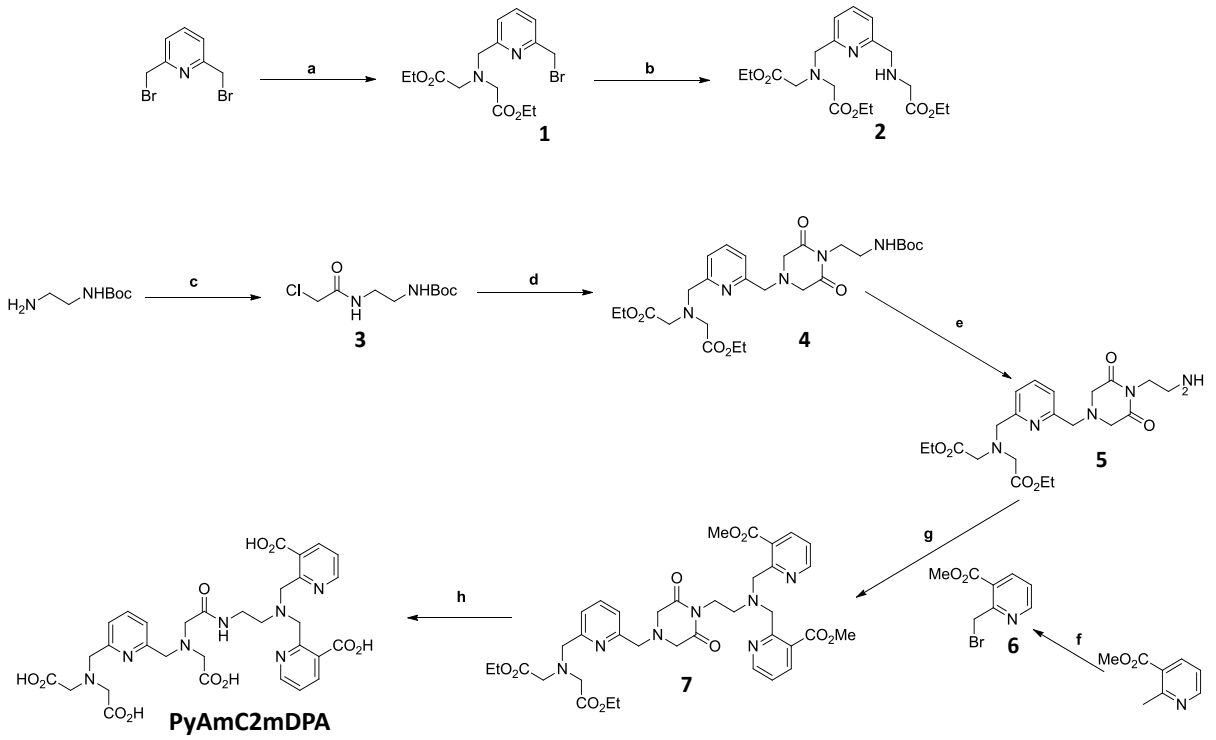

Scheme 2: Synthesis of ligand **PyAmC2mDPA**. Reagents and conditions: (a) diethyl iminodiacetate, K_2CO_3, CH_3CN, reflux, 87 %; (b) Glycine ethyl ester hydrochloride, K_2CO_3, NaI, CH_3CN, reflux, 71 %; (c) Chloroacetyl chloride, K_2CO_3, CH_3CN, rt; 80 % (d) **2**, K_2CO_3, NaI, CH_3CN, reflux, 87 %; (e) TFA, CH_2Cl_2, rt, quant.; (f) N-Bromosuccinimide, AIBN, $CHCl_3$, reflux, 42 %; (g) **6**, K_2CO_3, CH_3CN, reflux, 38 %; (h) LiOH, THF/H_2O (1 :1 v/v), rt, 90 %..

ZP1 and **ZP2** were both synthesized in three steps from n-propylamine (see Scheme S1, ESI). Successive nucleophilic substitution reactions of ethyl bromoacetate and 2-(chloromethyl)pyridine hydrochloride with n-propylamine, followed by a hydrolysis of the ester functions, afforded **ZP1**. **ZP2** was obtained by N-dialkylation of the n-propylamine with ethyl 2-(bromomethyl)nicotinate, obtained after a radical bromination of ethyl-2-methylnicotinate, followed by a final hydrolysis step.

Protonation constants of the ligands and stability constants of the complexes

Protonation constants, as defined in equation (1), were determined by pH-potentiometric titrations for **PyAmC2mDPA** (Figure 1) and **ZP2** (Figure S1). The results are reported in Table 1. **ZP2** shows three protonation constants in the pH range used for the measurements, the first one (9.50) corresponding to the

protonation of the nitrogen atom of the amine function, and the others to the carboxylate functions and/or the pyridine nitrogen.

PyAmC2mDPA displays six protonation constants, the first three related to the protonation of nitrogens from amine functions. By comparison with **ZP2**, **Py** and **L3**, the highest protonation constant can be attributed to the tertiary amine of the Zn^{2+}-binding moiety, while log K_{H2} corresponds to the protonation of the tertiary amine of the Gd^{3+} complexing part, and log K_{H3} to the nitrogen atom being close to the amide function. It has been previously observed that the vicinity of amide functions lowers the protonation constants,[25] and this is consistent with what is observed for **L3**. Finally, the last three protonation steps occur on carboxylate functions and the pyridinic nitrogens of the **ZP2** moiety.

Table 1. Protonation constants measured in KCl (0.1 M) at 298 K

Log K_H	PyAmC2mDPA	ZP2	PyC4mDPA[a]	L3[b]	Py[c]
Log K_{H1}	8.98(2)	9.50(6)	10.53(9)	8.80	8.95
Log K_{H2}	8.22(5)	3.6(1)	8.75(6)	7.93	7.85
Log K_{H3}	5.73(8)	2.90(9)	8.04(4)	5.55	3.38
Log K_{H4}	3.53(9)		3.79(5)	3.50	2.48
Log K_{H5}	2.64(3)		2.81(6)	2.4	
Log K_{H6}	2.14(3)		2.40(9)		
Log K_{H7}			1.9(1)		
Σ Log K_H	31.24	16	38.22	28.18	22.66

[a] From ref [26] [b] From ref [25]; [c] From ref [22]

$$K_i = \frac{[H_iL]}{[H_{i-1}L][H]} \quad (1)$$

$$K_{MmL} = \frac{[M_mL]}{[M_{m-1}L][\mathrm{M}]} \quad (2)$$

$$K_{MmLHi} = \frac{[M_mL]}{[M_mLH_{i-1}][H]} \quad (3)$$

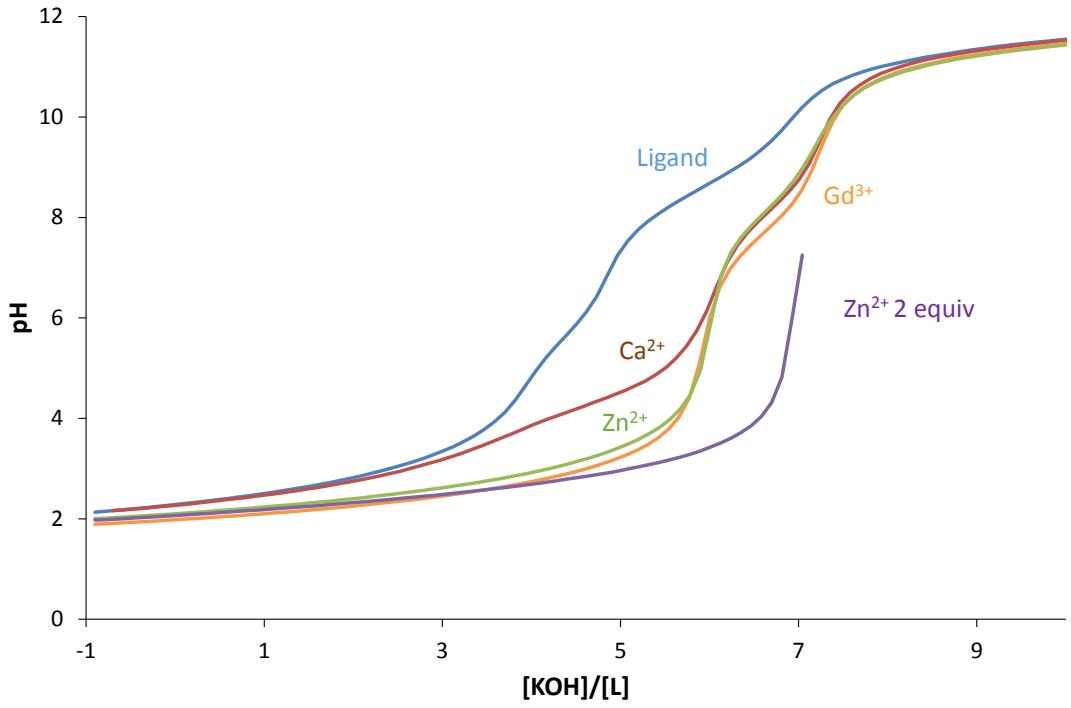

Figure 1: Potentiometric titration curves of solutions containing 2.92 mM **PyAmC2mDPA** with 0 or 1 equivalent of Ca^{2+}, Zn^{2+}, Gd^{3+} and 2 equivalents of Zn^{2+} in H_2O, 0.1 M KCl, 298 K.

Complex stability and protonation constants, log K_{ML} and log K_{MLH} (equations 2 and 3) have been determined for Gd^{3+} (Figure 1) by pH-potentiometric titration. The different species formed and their stability constants are summarized in Table 2. Gd^{3+} forms only mononuclear complexes with **PyAmC2mDPA** as previously observed for **L3**[25] and **PyC4mDPA**.[26]

The stability constant of **GdPyAmC2mDPA** is 16.27, which is lower than that of **GdPy** or **GdPyC4mDPA.** It was expected as a coordinating carboxylate group has been replaced by an amide function. The stability constant is one order of magnitude higher than that of **GdL3** due to the higher basicity of **PyAmC2mDPA** compared to **L3**. The three protonation constants observed for **GdPyAmC2mDPA** correspond to the protonation of the **ZP2** moiety on the tertiary amine, pyridine and/or carboxylate functions. The values of the stability and the three protonation constants confirm that Gd^{3+} is complexed within the "Gd^{3+}-binding pocket".

Table 2. Stability constants of the different complexes measured by potentiometric titration in KCl (0.1M) at 298 K.

Log *K*	PyAmC2mDPA	ZP2	PyC4mDPA[a]	L3[b]	Py[c]
Log K_{GdL}	16.27 (8)	-	20.1	15.15	18.60
Log K_{GdLH}	7.24 (7)	-	8.92	7.69	-
Log K_{GdLH2}	3.26 (5)	-	3.74	3.68	-
Log K_{GdLH3}	2.56 (4)	-	2.54	-	-
Log K_{CaL}	8.90 (6)	-	10.22	8.05	9.43
Log K_{CaLH}	7.89 (3)	-	9.86	8.10	-
Log K_{CaLH2}	4.55 (9)	-	5.0	-	-
Log K_{ZnL}	13.58 (9)	9.09 (3)	16.5	12.7	15.84
Log K_{ZnLH}	7.89 (3)	3.78 (3)	10.03	8.15	3.81
Log K_{ZnLH2}	3.72 (2)	-	4.10	3.90	-
Log K_{ZnLH3}	2.71 (2)	-	3.20	-	-
Log K_{ZnLH4}	2.27 (5)	-	2.4	-	-
Log K_{ZnLOH}	-	8.75 (4)	11.6	-	-
Log K_{ZnLOH2}	-	10.13 (4)	-		
Log K_{Zn2L}	8.3 (1)	-	9.9	8.10	-
Log K_{Zn2LH}	3.2 (1)	-	3.98	-	-
***p*Gd**[d]	14.83	-	17.34	14.52	17.44

[a] From ref [26] [b] From ref [25]; [c] From ref [22]; [d] Logarithmic concentration of the free gadolinium ion (*p*Ln = - Log$[Ln]_{free}$), calculated for [Ln] = 10^{-6} M, [L] = 10^{-5} M at pH = 7.4

The *in vivo* toxicity of Ln^{3+} complexes is related to the potential release of the free metal ion, which can be a consequence of transmetalation/transchelation occuring with endogenous cations/ligands[31]. Therefore, the stability constants of the complexes formed with endogenous cations such as Ca^{2+}, Zn^{2+} and Cu^{2+} have been assessed (Tables 2, S1-S2, and Figure 1, S1-S5 ESI). For Ca^{2+}, only the formation of a mononuclear complex is observed with **PyAmC2mDPA**. This is consistent with the fact that the stability constant of **CaZP2** is too low to be determined (Figure S2, ESI). So, the complexation of Ca^{2+} takes place in the "Gd^{3+}-binding moiety" and the values found are similar to that of **CaL3**. Again, the protonation steps observed occur on the **ZP2** moiety.

With Zn^{2+}, **PyAmC2mDPA** forms mono- and dinuclear complexes (Table 2). The first stability constant is close to that of **ZnL3**, and the four protonation constants observed correspond to protonation of the **ZP2** moiety as well as of the "Py pocket", as previously detected for **ZnPy**.[22] The stability constant of the dinuclear complex is

similar to those of **ZnZP2** (Figure S1, ESI) or **ZnDPA** (7.57).[32] This confirms that the first Zn^{2+} enters the "Gd^{3+}-binding moiety" and the second Zn^{2+} ion binds to the **ZP2** moiety. Importantly, Log K_{ZnL} is 3 orders of magnitude lower than Log K_{GdL}, showing that, thermodynamically, Zn^{2+} will not displace Gd^{3+}.

Due to the high affinity of Cu^{2+} for polyaminocarboxylate ligands,[33-35] UV-Visible data are often required in complement to potentiometric titrations. A complex stability constant of 17.63 was previously determined for **CuPy** using this method.[33] The UV-visible spectra of **CuZP2** (Figure S4) show complex formation even in 2 M HCl (pH = -0.3), preventing any precise determination of the stability constant. Thus, **CuZP2** has higher stability than **CuPy** or **CuL3**. For **CuPyAmC2mDPA** as well, the UV-visible spectra show complex formation at 1 M HCl, in the presence of one or two equivalents of Cu^{2+} (Figures S5, ESI), proving very high stability which prevents determination of the stability constants. Similar results were obtained with **CuPyC4mDPA** (Figure S6, ESI). In overall, as the stability constants of **CuZP2**, **CuPyAmC2mDPA** or **CuPyC4mDPA** are higher than that of **CuPy**, it can be suggested that the first Cu^{2+} is complexed by the **ZP2** moiety and the second by the "Gd^{3+}-binding moiety".

Relaxometric properties of the Gd^{3+} complex

The ^{1}H NMRD profiles of **GdPyAmC2mDPA** were recorded at three temperatures to characterize the parameters governing proton relaxivity (Figure S7, ESI). The relaxivity of **GdPyAmC2mDPA** is 13.6 $mM^{-1}.s^{-1}$ at 20 MHz and 298 K. It decreases with increasing temperature, which is classical for small molecular weight systems where rotation limits the relaxivity. These profiles are very similar to those of **GdL3,**[25] suggesting the presence of two water molecules in the first coordination sphere of Gd^{3+}.

To determine the microscopic parameters characterizing the structure and dynamics of the complex, the ^{1}H NMRD profiles were analyzed using the Solomon-Bloembergen and Morgan (SBM) theory. The rate, k_{ex}, and the activation enthalpy, $\Delta H^{\neq}$, of water exchange have been fixed to the values previously determined for **GdL3**.[25] The rotational correlation time, τ_R^{298}, of **GdPyAmC2mDPA** (Tables 3 and S3, and Figure S7 ESI) is 208 ps, consistent with the size of the complex as compared to **GdPy**, **GdPyC4mDPA** and **GdL3**.

Table 3. Parameters obtained from the fit of NMRD profiles at 298 K, 310 K and 323 K using the Solomon-Bloembergen and Morgan (SBM) theory.

	GdPyAmC2mDPA	**GdPyC4mDPA**[a]	**GdPy**[b]	**GdL3**[c]
$\Delta H^{\neq}$ (kJ.mol^{-1})[d]	47.3	50.4	50.4	47.3
k_{ex}^{298} (10^6 s^{-1})[d]	3.3	9.3	9.3	3.3
τ_R^{298} (ps)	208 (4)	185	92[e]	147[d]
E_r (kJ.mol^{-1})	23 (1)	21	20.2	26.1

a. From ref [27], b. From ref[22]; c. From ref [25], d. Fixed during the fitting procedure; e. τ_{RO} calculated from ^{17}O T_1 relaxation times

In order to study the influence of Zn^{2+} on the relaxometric properties of the complexes, the relaxivity of **GdPyAmC2mDPA** was monitored upon Zn^{2+} addition at 20 MHz and 298 K in 0.1 M HEPES (pH = 7.4) (Figure S8, ESI). The lack of any significant variation means that none of the parameters influencing relaxivity are modified in the presence of Zn^{2+}. For **GdPyC4mDPA,** relatively similar results are obtained, except for a slight, *ca.* 10 %, relaxivity increase upon addition of 1 eq. of Zn^{2+}.[26] This small increase cannot be attributed to a change in the Gd^{3+} coordination sphere, as the luminescence lifetime on the **EuPyC4mDPA** analogue does not vary upon addition of 1 eq. of Zn^{2+}.[26] Further, aggregate formation, which could also lead to r_1 increase, was excluded by the linear dependence of the paramagnetic relaxation rates, R_{1para}, on [**Zn-GdPyC4mDPA**] concentration (Figure S9, ESI). Luminescence titration of **EuPyC4mDPA** with Zn^{2+} (Figure S10, ESI) evidences a quenching of *ca.* 30% in the presence of one equivalent of Zn^{2+}. As the number of inner sphere water molecules remains constant upon Zn^{2+} binding, the luminescence quenching (for **EuPyC4mDPA**) and the relaxivity increase (for **GdPyC4mDPA**) observed both suggest that additional, second sphere water molecule(s) are likely present in the vicinity of the Ln^{3+} when Zn^{2+} is bound. Interestingly, such second sphere water molecules are less, present for **LnPyAmC2mDPA**.

This lack of relaxometric response to Zn^{2+} is very different from what was previously observed for **GdL3**. Indeed, a relaxivity increase of *ca.* 20% was obtained upon addition of 0.5 eq. of Zn^{2+}, ascribed to the formation of **Zn(GdL3)$_2$** dimer.[25] The main difference between the two series of complexes (**GdL2**/**GdL3** vs. **GdPyAmC2mDPA**/**GdPyC4mDPA**) lies in the Zn^{2+} chelating part. Potentiometric studies in presence of 0, 0.5, and 1eq. of Zn^{2+} were carried out on model compounds **ZP1** (for **GdL2/3**) and **ZP2** (for **GdPyAmC2mDPA/GdPyC4mDPA**, Figures S11-S15

and Table S2, ESI). Based on the data (Table 4), at pH 7.4, **Zn(ZP1)$_2$** has a 2.5 orders of magnitude higher conditional stability constant than **Zn(ZP2)$_2$**, implying that under the conditions of the relaxometric titrations, the dimer **Zn(ZP2)$_2$** represents less than 3% vs. over 70% for **Zn(ZP1)$_2$** (Figure 2). Even if the Zn^{2+}-GdL stability constants might slightly vary for **GdL3** and **GdPyAmC2mDPA** as compared to the model compounds, this large stability difference of the dinuclear complexes explains certainly why one can detect the formation of **Zn(GdL2)$_2$** and **Zn(GdL3)$_2$** in the relaxometric titration, but not that of **Zn(GdPyAmC2mDPA)$_2$** and **Zn(GdPyC4mDPA)$_2$**.

Table 4. Thermodynamic (Log K_{ZnL2}) and conditional (Log K_{cond}; at pH 7.4) stability constants at 0.1 M KCl; 298 K

	ZP1	**ZP2**
Log K_{ZnL2}	5.51 (3)	3.9 (2)
Log K_{cond}	4.35	1.80

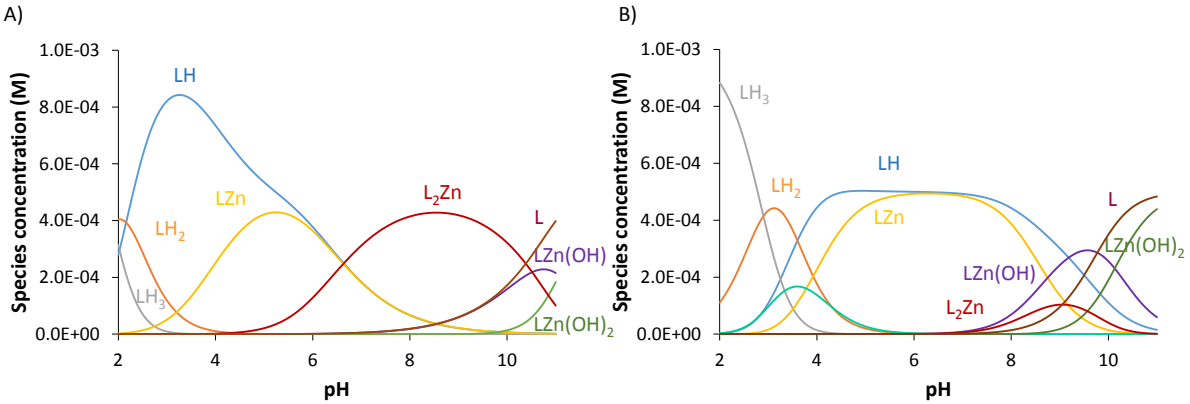

Figure 2: Species distribution of 1 mM of **ZP1** (A) or **ZP2** (B) in the presence of 0.5 mM of Zn^{2+}, calculated from the stability constant from Table S3.

The bishydrated state of both **GdPyC4mDPA** and **GdPyAmC2mDPA** led us conclude that the carboxylate function on the DPA pyridines does not bind to Gd^{3+}, and of course the lack of a relaxivity response to Zn^{2+} implies that the Gd^{3+} hydration number does not vary upon Zn^{2+} coordination. The non-coordination of these carboxylates is less surprising for the negatively charged **GdPyC4mDPA** core, but it could have occurred in the case of the neutral **GdPyAmC2mDPA**. Indeed, for the similarly neutral **GdL1** (Scheme 1), extra coordination from the Zn^{2+}-binding moieties was concluded based on the absence of hydration water in the complex.[25] In overall, these data

indicate that the position of the carboxylate on the pyridine, and probably even more importantly, the denticity of the Gd^{3+}-binding moiety are more determinant in this respect than the charge of the Gd^{3+} core.

Zinc detection in the presence of HSA

When a contrast agent is injected in the blood stream, it encounters many other molecules, in particular Human Serum Albumin (HSA), which is the most abundant protein and possesses a Zn-binding site.[36-37]

From potentiometric measurements, it can be inferred that the affinity of **GdPyAmC2mDPA** for Zn^{2+} (Log $K_{Zn2PyAmC2mDPA}$ = 8.3) is comparable to that of HSA (Log K_{ZnHSA} = 7.53).[18] As the Zn^{2+} coordination sphere is not complete neither in HSA,[38] nor in **GdPyAmC2mDPA**, ternary complexes of GdL-Zn-HSA could be formed. Moreover, due to the presence of several binding pockets in HSA, the complexes could bind to various sites.

We had previously shown that **GdPyC4mDPA**, which possesses the same **ZP2** binding moiety as **GdPyAmC2mDPA,** could detect Zn^{2+} in the presence of HSA.[26] The relaxivity increase observed in the presence of Zn^{2+} was due to HSA binding and not to a change in the hydration state of Gd^{3+},[27] thus we hypothesized a similar behaviour for **GdPyAmC2mDPA**.

To determine the number of HSA binding sites and their dissociation constants, two relaxometric titrations were performed: by increasing the concentration either of the Gd^{3+} complex (M-titration) or of HSA (E-titration). The M-titration (Figure 3A) shows that upon addition of up to 1.3 mM of **GdPyAmC2mDPA** or **GdPyAmC2mDPAZn** to a 0.6 mM of HSA solution, the Paramagnetic Relaxation Enhancement (PRE) increases without saturation which indicates that the interaction sites available on the HSA are not all occupied. From the concentration ratio, one can conclude that at least three sites are available for GdL binding. It should be noted that for **GdPyC4mDPA,** even higher concentrations have been used without saturation of the M-titration curve and suggested at least 5 interaction sites on the HSA.[26] Other Gd^{3+} chelates were previously reported to bind to more than one independent site with different binding constants.[39-40] Typically, these different binding constants are derived from ultrafiltration experiments, as relaxometric data alone do not allow for distinguishing between different binding models. These stepwise binding constants calculated from the ultrafiltration data show that one binding site is much stronger than the others. We therefore anticipated that the highest affinity site could be assessed from the E-

titration (Figure 3B), by considering a 1/1 binding isotherm and including experimental points only with HSA excess as compared to the complex.

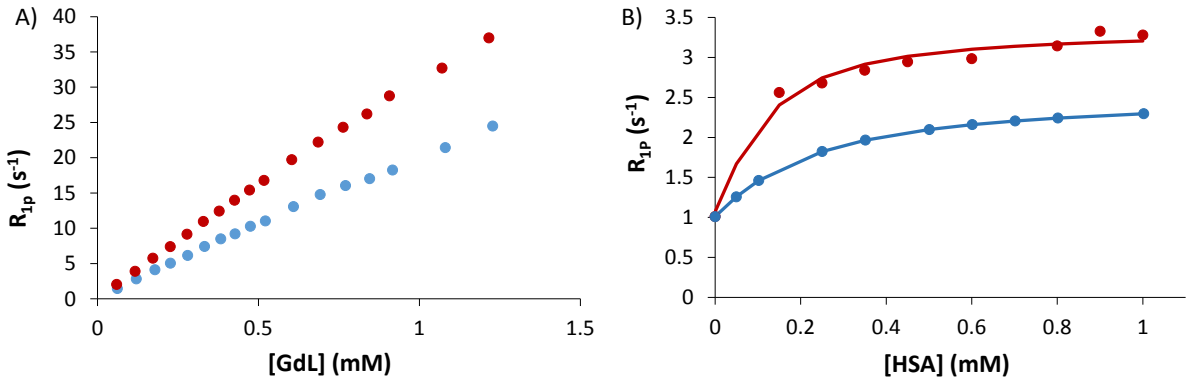

Figure 3: ^{1}H PRE measurements at pH = 7.4 (HEPES 0.1 M), 20 MHz, 310 K A) as a function of **GdPyAmC2mDPA** concentration in the presence of 0.6 mM of HSA and in the absence (blue) or in the presence (red) of 1 equivalent of Zn^{2+} (M titration); B) as a function of HSA concentration in the presence of [GdL4] = 0.10 mM in the absence (blue) or in the presence of 1 eq. of Zn^{2+} (red) (E titration). The solid curves represent the fit to eq. 8 with the parameters from Table 5 and S4.

Maximal values for the dissociation constants (K_D) can be obtained by fitting Paramagnetic Relaxation Enhancement (PRE) data to equation (8).

$$R_{1p} = 10^3 \times [(r_1^f . c_1) + \frac{1}{2}(r_1^b - r_1^f) \times (c_{HSA} + c_1 + K_D - \sqrt{(c_{HSA} + c_1 + K_D)^2 - 4c_{HSA}.c_1})] \quad (8)$$

Where r_1^f and r_1^b are the proton relaxivities of the free and bound (to HSA) complexes, c_{HSA} and c_1 are the concentration of HSA and the complex, respectively.

Fluorescence competitive experiments can also be performed using dansylglycine and dansylarginine as a competitor for site II and site I of HSA, respectively. The fluorescence of the dansyl part is increased and blue-shifted when bound to HSA.[41] The affinity of dansylglycine for site II was found to be 3.4 µM,[27] and the affinity of dansyl arginine for site I was found to be 125 µM (Figure S16, ESI), both in agreement with literature data.[42]

In order to decipher which part of the complex is responsible for HSA affinity, we performed:

(1) PRE measurements on **GdPyAmC2mDPA**, **GdPyAmC2mDPAZn** (Figure 3B) and **GdPy** (Figure S17).

(2) fluorescence competition experiments on **ZP2** and **ZnZP2** (Figure 4 and S18).

It was previously shown, for **GdPyC4mDPA,** that the affinity for site II determined by fluorescence was consistent with that measured by PRE in excess of HSA.[27]

Here, an increase in PRE is observed upon addition of HSA to **GdPyAmC2mDPA** or **GdPyAmC2mDPAZn**, while no significant increase is observed for **GdPy**. Concerning the fluorescence, addition of **ZP2** or **ZP2Zn** to an HSA/dansylglycine mixture results in a fluorescence decrease indicating a displacement of dansylglycine by the complexes. The decrease is much smaller with dansylarginine (Figure S18) indicating a smaller affinity for this site, as already reported for such systems.[36, 43] The dissociation constants, presented in Table 5, allow for several conclusions:

(3) The dissociation constant for **GdPyAmC2mDPA** is about two times lower with Zn^{2+} than without, in full accordance with previous data for **GdPyC4mDPA**.[27]

(4) The parent compound **GdPy** does not bind strongly to HSA.

(5) **ZP2** binds more strongly to site II than to site I of HSA

(6) There is no significant change in the affinity of **ZP2** for HSA whether Zn^{2+} is present or not.

The affinity **GdPyAmC2mDPAZn** for HSA is in the same order of magnitude to that of **GdPyC4mDPAZn**[27] and to those reported in the literature for other Zn-bound DPA-derivatives.[37] The fluorescence displacement measurements point out a binding of the complexes in the absence and in the presence of Zn^{2+} to site I and II of HSA, with a higher affinity for site II. Nevertheless, a binding to the MBS of HSA (higher affinity site for Zn^{2+}) cannot be excluded. Indeed, this binding could also affect site II of HSA, as a crosstalk between the two binding sites has already been demonstrated.[38, 44] Moreover, it should be pointed out that when bound to the DPA-unit, Zn^{2+} needs to conserve a free coordination site to allow for HSA binding. Indeed, we have previously evidenced the lack of specific HSA interaction for a modified DPA-moiety that saturates the Zn^{2+} coordination sphere.[45]

The very limited interaction observed between **GdPy** and HSA points out the importance of the Zn-binding moiety. On the other hand, the similar HSA affinity of **ZP2** and **ZnZP2** evidences that the “Gd core” also has a role, even if the **GdPyAmC2mDPA**-HSA interaction occurs through the Zn-binding part. The “Gd core” is necessary to trigger higher affinity in the presence of Zn^{2+} through additional interactions between HSA and the “Gd core”.

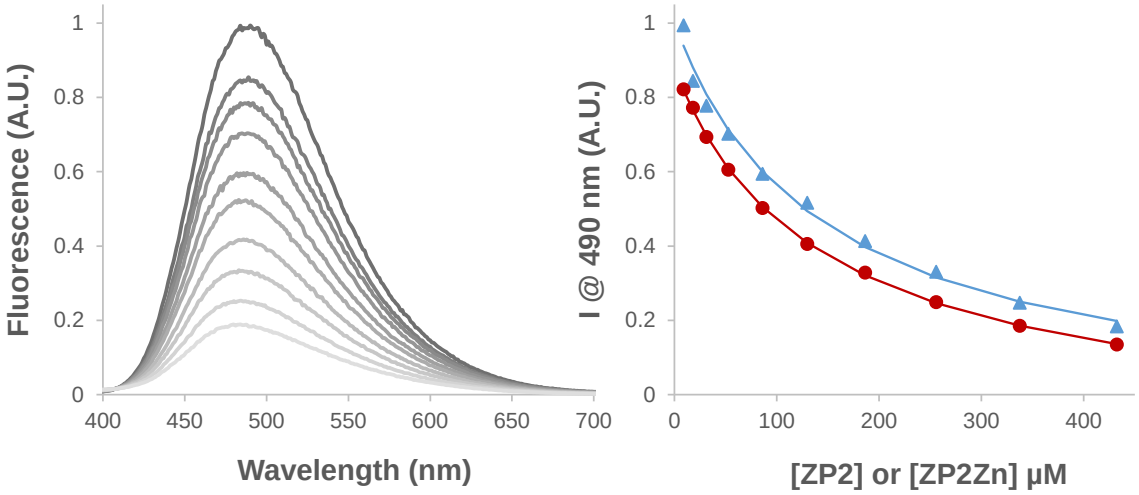

Figure 4: (Left) Fluorescence emission spectra of a solution of [HSA] = 5 µM (HEPES 0.1 M, pH = 7.4) and [Dansylglycine] = 10µM upon addition of **ZP2** after excitation at 260 nm. (Right) Emission intensity at 490 nm upon addition of **ZP2** (▲) or **ZP2Zn** (●) and the calculated intensities using HypSpec.

Table 5: Conditional dissociation constants (K_{D1}) measured by PRE and dissociation constants for site II ($K_{D\ site\ II}$) measured by fluorescence competition experiments, at 37°C and pH 7.4.

	K_D (µM) (PRE)	**$K_{D\ site\ II}$ (µM)** (Fluorescence)
GdPy	Non specific	-
ZP2	-	37 (10)
ZP2Zn		33 (10)
GdPyAmC2mDPA	170 (50)	-
GdPyAmC2mDPAZn	60 (20)	-
GdPyC4mDPA[a]	60	45
GdPyC4mDPAZn[a]	30	25

a. From ref [27]

Finally, the structure of the "Gd core", and certainly its charge, plays a crucial role in the affinity as illustrated by the difference of affinity of **GdPyAmC2mDPA** and **GdPyC4mDPA** for HSA. This is not surprising as drug binding sites are hydrophobic pockets with cationic residues at their surface,[14] therefore the negatively charged "Gd

core" of **GdPyC4mDPA** should create additional electrostatic interactions, resulting in a stronger binding.

Finally, due to the difference of affinity for HSA, more **GdPyAmC2mDPA** is bound to HSA in the presence of Zn^{2+} which explains the relaxivity increase.

Next, the NMRD profiles of **GdPyAmC2mDPA** in the presence of physiological concentration of HSA were recorded in the absence and in the presence of 1 eq. of Zn^{2+} at 25°C and 37°C (Figure S19). A hump is observed at intermediate magnetic fields, which is typical of slowly rotating species, confirming the interaction of the complexes with HSA both in the absence and in the presence of Zn^{2+}.

In the conditions used for these experiments, and knowing the affinity of **GdPyAmC2mDPA** for HSA at 37°C, nearly 70% of the complex is bound to HSA in the absence of Zn^{2+}, while it is more than 80% in the presence of Zn^{2+}. Using equation (8) with the affinity constant of **GdPyAmC2mDPA** for HSA (Table 6), and the relaxivities recorded in the absence of HSA (Figure S7), it is possible to recalculate the NMRD profile for the bound species both in the absence and in the presence of Zn^{2+} (Figure 5). These NMRD profiles at 37°C were fitted using the Solomon-Bloembergen and Morgan theory including the Lipari Szabo approach (equations in ESI). This approach takes into account local and global motions, characterized by a local rotational correlation time τ_l^{310} of the Gd^{3+} complex, and a global rotational correlation time τ_g^{310} of the whole system. The model-independent order parameter S^2 reflects the degree of spatial restriction of the local motion with respect to the global motion. Its value ranges from 0 to 1, referring respectively to an isotropic and a completely restricted internal motion. The fitting of the NMRD data has been restricted to frequencies above 4 MHz as at lower magnetic fields the SBM theory fails in describing electronic parameters and rotational dynamics of slowly rotating species. In the fitting process, the number of inner sphere water molecules has been fixed to 2, and the water exchange rate k_{ex}, as well as its activation enthalpy have been fixed to $3.3.10^6$ s^{-1} and 47.3 $kJ.mol^{-1}$ which corresponds to the values determined for **GdL3**.[25]

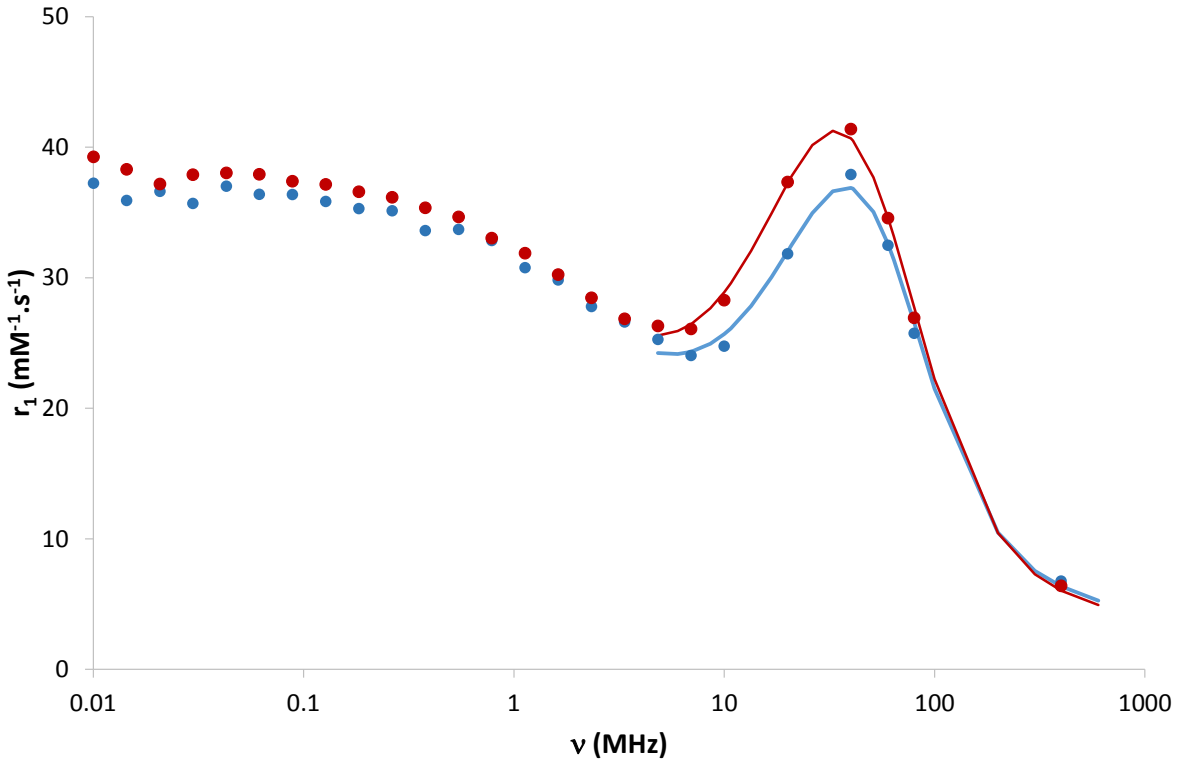

Figure 5: Calculated NMRD profiles of **GdPyAmC2mDPA** (●) and **GdPyAmC2mDPAZn** (●) at 37°C in the presence of 0.6 mM of HSA at pH 7.4 (HEPES 0.1 M). K_D from Table 5, experimental NMRD profiles from Figure S19 and Figure S7 were taken into account for the calculations. The lines represent the best fit to the SBM theory using the Lipari-Szabo approach.

The resulting parameters are presented in Table 6 and S5, and several conclusions can be drawn from these fittings. First, the values of local and global correlation times are not affected upon Zn^{2+} binding. The values of global rotational correlation times are lower than those typically found for HSA (20 ns) and measured by deuterium relaxation rate of small molecules strongly bound to HSA.[46] They are, however, fully consistent with values determined from the fitting of NMRD profiles including high fields points (> 100 MHz) for BSA[47] and HSA[48-49]. Importantly, upon Zn^{2+} binding, the S^2 parameter is increased, showing that the system becomes more rigid. Finally, τ_l^{310}, τ_l^{310} and S^2 are significantly higher for **GdPyAmC2mDPA** than for **GdPyC4mDPA** (Table 6),[27] which can be explained by the different size and nature of the linker. At 37°C and 40 MHz in the presence of 0.6 mM of HSA, **GdPyAmC2mDPA** shows a *ca.* 10% relaxivity increase upon Zn^{2+} binding. This limited increase is due to the rigidity of the system already in the absence of Zn^{2+} as reflected by the high S^2.

We should note that an eventual decrease of the water exchange rate upon HSA binding cannot be excluded, as it has been previously observed.[50] Unfortunately, it is

not possible to measure k_{ex} by ^{17}O NMR on the HSA-bound chelate, since the sample cannot be sufficiently concentrated and there is always a mixture of the bound and unbound chelate. The temperature-dependency of the relaxivities indicates that in the absence of Zn^{2+}, relaxivity remains limited by rotation. In the presence of Zn^{2+}, relaxivities are similar at 25°C and 37°C, suggesting that water exchange might potentially limit relaxivity.

In order to ascertain that the conclusions of the NMRD analysis of the HSA-bound systems remain valid even if there is a k_{ex} decrease upon HSA binding, we have re-fitted the profiles by assuming lower k_{ex} values. We obtained identical tendency for both cases, i.e. in the presence or in the absence of Zn : Upon increasing k_{ex} by 50 %, there are no significant variations in any of the rotational parameters. When decreasing k_{ex} by 50%, the rotational correlation time remains the same, and the S^2 parameter increases by ca. 15 %. Therefore, under the reasonable assumption that the decrease (if any) of the GdL water exchange rate upon HSA binding is not strongly affected by the presence of Zn^{2+}, our conclusion remains valid: the analysis of the NMRD curves evidences that the presence of Zn^{2+} leads to an increase of the parameter S^2, thus an increase of the rigidity of the system.

Table 6: Parameters obtained from the fitting of the NMRD profiles in the presence of HSA using Lipari-Szabo approach

	GdPyAmC2mDPA	**GdPyAmC2mDPAZn**	**GdPyC4mDPA[a]**	**GdPyC4mDPAZn[a]**
τ_g^{310} **(ps)**	2500[b]	2500[b]	2300(200)	2200(200)
τ_l^{310} **(ps)**	100(40)	90(20)	78(4)	65(9)
S^2	0.38(1)	0.42(1)	0.14(1)	0.21(1)

[a] From ref [27]; [b] Fixed during the fitting procedure

Conclusion

To conclude, we have synthesized and characterized a novel Gd^{3+} complex, **GdPyAmC2mDPA**, possessing a DPA-type "zinc binding moiety". Potentiometric titrations have shown a good selectivity of the Gd^{3+}-binding pocket for Gd^{3+} vs Zn^{2+}. The thermodynamic stability of **GdPyAmC2mDPA** remains modest, and as expected, several orders of magnitude lower than its analogue where the amide is replaced by a carboxylic function. However, it allows fundamental *in vitro* studies in order to decipher

the key parameters playing a role in Zn^{2+} detection. We have shown that the structure of the Zn^{2+}-binding unit is crucial to avoid $(GdL)_2Zn$ dimer formation. On the other hand, the carboxylate functions present on the DPA do not coordinate to the Gd^{3+}. Therefore, the relaxometric properties of **GdPyAmC2mDPA** are not modified upon Zn^{2+} addition.

The *in vitro* detection of Zn^{2+} is possible in presence of HSA as a significant relaxivity increase is obtained at intermediate fields (20-60 MHz) upon Zn^{2+} complexation. We show that the complex binds to HSA even in the absence of Zn^{2+}. The relaxivity response obtained in the presence of Zn^{2+} is due to a twofold higher affinity for HSA. The complexes have a stronger binging to site II compared to site I of HSA. The affinity of **GdPyAmC2mDPA** for HSA is guided by the Zn^{2+}-binding moiety but interestingly the “Gd-core” also plays a key role in the difference of affinity for Zn^{2+}.

The fit of the variable field relaxivity data using the Lipari-Szabo approach evidenced that the system is more rigid in the presence of Zn^{2+}, certainly explained by a different binding mode. The short linker between the “Gd-core” and the Zn-binding pocket results in a moderate relaxivity increase at medium fields, as the rigidity in the absence of Zn^{2+} is already high.

These fundamental insights obtained both on the relationship between the structure and relaxivity response of Zn^{2+} responsive Gd^{3+} probes and on their HSA interactions are important to understand their *in vitro* and *in vivo* behaviour. This information will be also helpful for the future design of improved contrast agents for Zn^{2+} detection.

Acknowledgements

We thank the Mo2ving platform for NMR and mass spectrometry characterisation. We acknowledge the support from Agence Nationale pour le recherche (grant ANR-13-JS07-0007), ITMO Cancer of Aviesan within the framework of 2021-2030 cancer control strategy on funds administered by Inserm and La Ligue Contre le Cancer (Comités du Loiret, Loire et Cher, Eure et Loire and Morbihan, grants PM-FP/2021-407 and PM-FP/2020-244).This project has received funding from the European Union’s Horizon 2020 research and innovation program under the Marie Sklodowska-Curie grant agreement No 898850. Gy.T. thank the financial support for the Hungarian National Research, Development, and Innovation Office (NKFIH K-134694 project)

Supporting Information Available

Synthesis, potentiometric, relaxivity, UV and luminescence measurements, equations for the fit of the NMRD profiles.

Keywords: Molecular imaging • Zinc • Responsive • Gadolinium • MRI • Human Serum Albumin

References

1. Que, E. L.; Domaille, D. W.; Chang, C. J., Metals in neurobiology: Probing their chemistry and biology with molecular imaging. *Chem. Rev.* **2008,** *108* (5), 1517-1549.
2. Berg, J. M.; Shi, Y. G., The galvanization of biology: A growing appreciation for the roles of zinc. *Science* **1996,** *271* (5252), 1081-1085.
3. Nishida, K.; Uchida, R., Role of Zinc Signaling in the Regulation of Mast Cell-, Basophil-, and T Cell-Mediated Allergic Responses. *Journal of Immunology Research* **2018,** *2018*, 5749120.
4. Que, E. L.; Bleher, R.; Duncan, F. E.; Kong, B. Y.; Gleber, S. C.; Vogt, S.; Chen, S.; Garwin, S. A.; Bayer, A. R.; Dravid, V. P.; Woodruff, T. K.; O'Halloran, T. V., Quantitative mapping of zinc fluxes in the mammalian egg reveals the origin of fertilization-induced zinc sparks. *Nature Chemistry* **2015,** *7* (2), 130-139.
5. Kelleher, S. L.; McCormick, N. H.; Velasquez, V.; Lopez, V., Zinc in Specialized Secretory Tissues: Roles in the Pancreas, Prostate, and Mammary Gland. *Adv. Nutr.* **2011,** *2* (2), 101-111.
6. Faller, P.; Hureau, C., A Bioinorganic View of Alzheimer's Disease: When Misplaced Metal Ions (Re)direct the Electrons to the Wrong Target. *Chem. Eur. J.* **2012,** *18* (50), 15910-15920.
7. Myers, S. A., Zinc transporters and zinc signaling: new insights into their role in type 2 diabetes. *Int. J. Endocrinol.* **2015,** *2015*, 167503-167503.
8. Bonnet, C. S.; Tei, L.; Botta, M.; Toth, E., Responsive probes. In *The Chemistry of Contrast Agents in Medical Magnetic Resonance Imaging*, Merbach, A. E.; Helm, L.; Toth, E., Eds. John Wiley & Sons: Chichester, 2013; pp 343-385.
9. Bonnet, C. S., Zn2+ detection by MRI using Ln3+-based complexes: The central role of coordination chemistry. *Coord. Chem. Rev.* **2018,** *369*, 91-104.
10. Malikidogo, K. P.; Martin, H.; Bonnet, C. S., From Zn(II) to Cu(II) Detection by MRI Using Metal-Based Probes: Current Progress and Challenges. *Pharmaceuticals* **2020,** *13* (12), 436.
11. Jordan, M. V. C.; Lo, S.-T.; Chen, S.; Preihs, C.; Chirayil, S.; Zhang, S.; Kapur, P.; Li, W.-H.; De Leon-Rodriguez, L. M.; Lubag, A. J. M.; Rofsky, N. M.; Sherry, A. D., Zinc-sensitive MRI contrast agent detects differential release of Zn(II) ions from the healthy vs. malignant mouse prostate. *PNAS* **2016,** *113* (37), E5464-E5471.

12. Lubag, A. J. M.; De Leon-Rodriguez, L. M.; Burgess, S. C.; Sherry, A. D., Noninvasive MRI of beta-cell function using a Zn2+-responsive contrast agent. *PNAS* **2011,** *108* (45), 18400-18405.
13. Khalighinejad, P.; Parrott, D.; Sherry, A. D., Imaging Tissue Physiology In Vivo by Use of Metal Ion-Responsive MRI Contrast Agents. *Pharmaceuticals* **2020,** *13* (10), 268.
14. He, X. M.; Carter, D. C., Atomic structure and chemistry of human serum albumin. *Nature* **1992,** *358* (6383), 209-215.
15. Fanali, G.; di Masi, A.; Trezza, V.; Marino, M.; Fasano, M.; Ascenzi, P., Human serum albumin: From bench to bedside. *Molecular Aspects of Medicine* **2012,** *33* (3), 209-290.
16. Bal, W.; Sokolowska, M.; Kurowska, E.; Faller, P., Binding of transition metal ions to albumin: Sites, affinities and rates. *Biochimica Et Biophysica Acta-General Subjects* **2013,** *1830* (12), 5444-5455.
17. Blindauer, C. A.; Harvey, I.; Bunyan, K. E.; Stewart, A. J.; Sleep, D.; Harrison, D. J.; Berezenko, S.; Sadler, P. J., Structure, Properties, and Engineering of the Major Zinc Binding Site on Human Albumin *. *J. Biol. Chem.* **2009,** *284* (34), 23116-23124.
18. Masuoka, J.; Hegenauer, J.; Van Dyke, B. R.; Saltman, P., Intrinsic stoichiometric equilibrium constants for the binding of zinc(II) and copper(II) to the high affinity site of serum albumin. *J. Biol. Chem.* **1993,** *268* (29), 21533-7.
19. Van Biervliet, S.; Van Biervliet, J. P.; Vande Velde, S.; Robberecht, E., Serum zinc concentrations in cystic fibrosis patients aged above 4 years: a cross-sectional evaluation. *Biol. Trace Elem. Res.* **2007,** *119* (1), 19-26.
20. Caille, F.; Bonnet, C. S.; Buron, F.; Villette, S.; Helm, L.; Petoud, S.; Suzenet, F.; Toth, E., Isoquinoline-Based Lanthanide Complexes: Bright NIR Optical Probes and Efficient MRI Agents. *Inorg. Chem.* **2012,** *51* (4), 2522-2532.
21. Bonnet, C. S.; Buron, F.; Caille, F.; Shade, C. M.; Drahos, B.; Pellegatti, L.; Zhang, J.; Villette, S.; Helm, L.; Pichon, C.; Suzenet, F.; Petoud, S.; Toth, E., Pyridine-Based Lanthanide Complexes Combining MRI and NIR Luminescence Activities. *Chem. Eur. J.* **2012,** *18* (5), 1419-1431.
22. Pellegatti, L.; Zhang, J.; Drahos, B.; Villette, S.; Suzenet, F.; Guillaumet, G.; Petoud, S.; Toth, E., Pyridine-based lanthanide complexes: towards bimodal agents operating as near infrared luminescent and MRI reporters. *Chem. Commun.* **2008,** (48), 6591-6593.
23. Lacoste, R. G.; Christof.Gv; Martell, A. E., NEW MULTIDENTATE LIGANDS .2. AMINO ACIDS CONTAINING ALPHA-PYRIDYL GROUPS. *J. Am. Chem. Soc.* **1965,** *87* (11), 2385-2388.
24. Hanaoka, K.; Kikuchi, K.; Urano, Y.; Narazaki, M.; Yokawa, T.; Sakamoto, S.; Yamaguchi, K.; Nagano, T., Design and synthesis of a novel magnetic resonance imaging contrast agent for selective sensing of zinc ion. *Chem. Biol.* **2002,** *9* (9), 1027-1032.
25. Bonnet, C. S.; Caille, F.; Pallier, A.; Morfin, J.-F.; Petoud, S.; Suzenet, F.; Toth, E., Mechanistic Studies of Gd3+-Based MRI Contrast Agents for Zn2+ Detection: Towards Rational Design. *Chem. Eur. J.* **2014,** *20* (35), 10959-10969.
26. Malikidogo, K. P.; Da Silva, I.; Morfin, J.-F.; Lacerda, S.; Barantin, L.; Sauvage, T.; Sobilo, J.; Lerondel, S.; Tóth, É.; Bonnet, C. S., A cocktail of 165Er(iii) and Gd(iii) complexes for quantitative detection of zinc using SPECT and MRI. *Chem. Commun.* **2018,** *54* (55), 7597-7600.
27. Malikidogo, K. P.; Isaac, M.; Uguen, A.; Même, S.; Pallier, A.; Morfin, J.-F.; Lacerda, S.; Toth, E.; Bonnet, C. S., Zinc-sensitive MRI contrast agents: Importance of local probe accumulation in Zinc-rich tissues. *submitted*.
28. Martell, A. E.; Motekaitis, R. J., *Determination and use of stability constants*. VCH: 1992.

29. Gans, P.; Sabatini, A.; Vacca, A., Investigation of equilibria in solution. Determination of equilibrium constants with the HYPERQUAD suite of programs. *Talanta* **1996,** *43* (10), 1739-1753.
30. Raiford, D. S.; Fisk, C. L.; Becker, E. D., Calibration of Methanol and Ethylene-Glycol Nuclear Magnetic-Resonance Thermometers. *Anal. Chem.* **1979,** *51* (12), 2050-2051.
31. Cacheris, W. P.; Quay, S. C.; Rocklage, S. M., The Relationship between Thermodynamics and the Toxicity of Gadolinium Complexes. *Magn. Reson. Imaging* **1990,** *8* (4), 467-481.
32. Romary, J. K.; Barger, J. D.; Bunds, J. E., New multidentate alpha-pyridyl ligand. Coordination of bis(2-pyridylmethyl)amine with transition metal ions. *Inorg. Chem.* **1968,** *7* (6), 1142-1145.
33. Bonnet, C. S.; Laine, S.; Buron, F.; Tircso, G.; Pallier, A.; Helm, L.; Suzenet, F.; Toth, E., A Pyridine-Based Ligand with Two Hydrazine Functions for Lanthanide Chelation: Remarkable Kinetic Inertness for a Linear, Bishydrated Complex. *Inorg. Chem.* **2015,** *54* (12), 5991-6003.
34. Rodriguez-Rodriguez, A.; Garda, Z.; Ruscsak, E.; Esteban-Gomez, D.; de Blas, A.; Rodriguez-Blas, T.; Lima, L. M. P.; Beyler, M.; Tripier, R.; Tircso, G.; Platas-Iglesias, C., Stable Mn2+, Cu2+ and Ln3+ complexes with cyclen-based ligands functionalized with picolinate pendant arms. *Dalton Trans.* **2015,** *44* (11), 5017-5031.
35. Regueiro-Figueroa, M.; Ruscsák, E.; Fra, L.; Tircsó, G.; Tóth, I.; de Blas, A.; Rodríguez-Blas, T.; Platas-Iglesias, C.; Esteban-Gómez, D., Highly Stable Complexes of Divalent Metal Ions (Mg2+, Ca2+, Cu2+, Zn2+, Cd2+, and Pb2+) with a Dota-Like Ligand Containing a Picolinate Pendant. *Eur. J. Inorg. Chem.* **2014,** *2014* (36), 6165-6173.
36. Esqueda, A. C.; Lopez, J. A.; Andreu-De-Riquer, G.; Alvarado-Monzon, J. C.; Ratnakar, J.; Lubag, A. J. M.; Sherry, A. D.; De Leon-Rodriguez, L. M., A New Gadolinium-Based MRI Zinc Sensor. *J. Am. Chem. Soc.* **2009,** *131* (32), 11387-11391.
37. Yu, J.; Martins, A. F.; Preihs, C.; Clavijo Jordan, V.; Chirayil, S.; Zhao, P.; Wu, Y.; Nasr, K.; Kiefer, G. E.; Sherry, A. D., Amplifying the Sensitivity of Zinc(II) Responsive MRI Contrast Agents by Altering Water Exchange Rates. *J. Am. Chem. Soc.* **2015,** *137* (44), 14173-14179.
38. Coverdale, J. P. C.; Barnett, J. P.; Adamu, A. H.; Griffiths, E. J.; Stewart, A. J.; Blindauer, C. A., A metalloproteomic analysis of interactions between plasma proteins and zinc: elevated fatty acid levels affect zinc distribution†. *Metallomics* **2019,** *11* (11), 1805-1819.
39. Caravan, P.; Cloutier, N. J.; Greenfield, M. T.; McDermid, S. A.; Dunham, S. U.; Bulte, J. W. M.; Amedio, J. C.; Looby, R. J.; Supkowski, R. M.; Horrocks, W. D.; McMurry, T. J.; Lauffer, R. B., The Interaction of MS-325 with Human Serum Albumin and Its Effect on Proton Relaxation Rates. *J. Am. Chem. Soc.* **2002,** *124* (12), 3152-3162.
40. Moriggi, L.; Yaseen, M. A.; Helm, L.; Caravan, P., Serum Albumin Targeted, pH-Dependent Magnetic Resonance Relaxation Agents. *Chem. Eur. J.* **2012,** *18* (12), 3675-3686.
41. Lakowicz, J. R., *Principles of Fluorescence Spectroscopy*. Springer: 2006; p 954.
42. Bertozo, L. d. C.; Maszota-Zieleniak, M.; Bolean, M.; Ciancaglini, P.; Samsonov, S. A.; Ximenes, V. F., Binding of fluorescent dansyl amino acids in albumin: When access to the protein cavity is more important than the strength of binding. *Dyes and Pigments* **2021,** *188*, 109195.
43. Xu, Y.-Q.; Luo, J.; Chen, Z.-N., Zn2+-Responsive Bimodal Magnetic Resonance Imaging and Fluorescence Imaging Agents and Their Interaction with Human Serum Albumin. *Eur. J. Inorg. Chem.* **2014,** (20), 3208-3215.
44. Martins, A. F.; Jordan, V. C.; Bochner, F.; Chirayil, S.; Paranawithana, N.; Zhang, S.; Lo, S.-T.; Wen, X.; Zhao, P.; Neeman, M.; Sherry, A. D., Imaging Insulin Secretion from

Mouse Pancreas by MRI Is Improved by Use of a Zinc-Responsive MRI Sensor with Lower Affinity for Zn2+ Ions. *J. Am. Chem. Soc.* **2018,** *140* (50), 17456-17464.
45. Wang, G.; Martin, H.; Amézqueta, S.; Ràfols, C.; Bonnet, C. S.; Angelovski, G., Insights into the Responding Modes of Highly Potent Gadolinium-Based Magnetic Resonance Imaging Probes Sensitive to Zinc Ions. *Inorg. Chem.* **2022,** *61* (41), 16256-16265.
46. Elst, L. V.; Laurent, S.; Bintoma, H. M.; Muller, R. N., Albumin-bound MRI contrast agents: the dilemma of the rotational correlation time. *Magnetic Resonance Materials in Physics, Biology and Medicine* **2001,** *12* (2), 135-140.
47. Tóth, É.; Connac, F.; Helm, L.; Adzamli, K.; Merbach, A. E., Direct assessment of water exchange on a Gd(III) chelate bound to a protein. *JBIC Journal of Biological Inorganic Chemistry* **1998,** *3* (6), 606-613.
48. Geraldes, C. F. G. C.; Sherry, A. D.; Vallet, P.; Maton, F.; Muller, R. N.; Mody, T. D.; Hemmi, G.; Sessler, J. L., Nuclear magnetic relaxation dispersion studies of water-soluble gadolinium(iii)-texaphyrin complexes. *Journal of Magnetic Resonance Imaging* **1995,** *5* (6), 725-729.
49. Muller, R. N.; Radüchel, B.; Laurent, S.; Platzek, J.; Piérart, C.; Mareski, P.; Vander Elst, L., Physicochemical Characterization of MS-325, a New Gadolinium Complex, by Multinuclear Relaxometry. *Eur. J. Inorg. Chem.* **1999,** *1999* (11), 1949-1955.
50. Aime, S.; Anelli, P.; Botta, M.; Brocchetta, M.; Canton, S.; Fedeli, F.; Gianolio, E.; Terreno, E., Relaxometric evaluation of novel manganese(II) complexes for application as contrast agents in magnetic resonance imaging. *JBIC Journal of Biological Inorganic Chemistry* **2002,** *7* (1), 58-67.

TOC

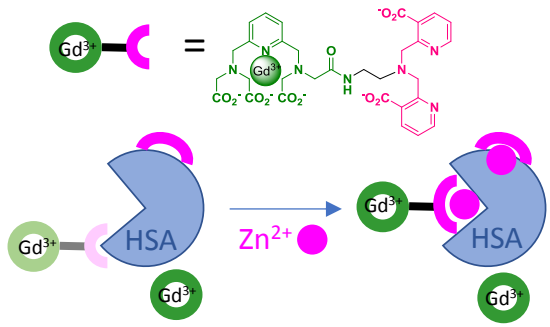

The in vitro relaxivity response of a Zn^{2+}-sensitive Gd^{3+} complex in the presence of HSA is explored through relaxivity, fluorescence and potentiometric measurements. The results are compared to those of analogous complexes to assess the molecular mechanism underlying the Zn^{2+} dependent relaxivity changes.